Slow Motion in the CAA·TTG Sequence of a DNA Decamer Duplex Studied by NMR†

Chojiro Kojima,‡,§ Nikolai B. Ulyanov,‡ Masatsune Kainosho,§,|| and Thomas L. James*,‡

Department of Pharmaceutical Chemistry, University of California, San Francisco, San Francisco, California 94143-0446, CREST, Japan Science and Technology Corporation, Kawaguchi, Saitama 332-0012, Japan, and Department of Chemistry, Graduate School of Science, Tokyo Metropolitan University, Hachioji, Tokyo 192-0397, Japan

Received February 15, 2001; Revised Manuscript Received April 24, 2001

ABSTRACT: In DNA duplexes, pyrimidine−purine steps are believed to be flexible or conformationally unstable. Indeed, several DNA crystal structures exhibit a multitude of conformations for CpA·TpG steps. The question arises of whether this structural flexibility is accompanied by dynamical flexibility, i.e., a question pertaining to the energy barrier between conformations. Except for TpA steps, slow motions on the microsecond-to-millisecond time scale have not been detected in duplexes until now. In the present study, such slow motion was investigated by ^{1}H, ^{13}C, and ^{15}N NMR relaxation measurements on a DNA decamer d(CATTTGCATC)·d(GATGCAAATG). The DNA decamer was enriched with 15% ^{13}C and 98% ^{15}N isotopes for each adenosine and guanosine residue. Three lines of evidence support the notion of slow motion in the CAA·TTG moiety. Analysis of ^{15}N relaxation showed that the order parameter, S^2, of guanosine imino NH groups was about 0.8, similar to that of CH groups for this oligomer. The strong temperature dependence of guanosine NH S^2 in the CAA·TTG sequence indicated the presence of a large-amplitude motion. Signals of adenosine H8 protons in the CAA·TTG sequence were broadened in 2D ^{1}H NOESY spectra, which also suggested the existence of slow motion. As well as being smaller than for other adenine residues, the ^{1}H T_2 values exhibited a magnetic field strength dependence for all adenosine H8 signals in the ATTTG·CAAAT region, suggesting slow motions more pronounced at the first adenosine in the CAA·TTG sequence but extending over the CAAAT·ATTTG region. This phenomenon was further examined by the pulse field strength dependence of the ^{1}H, ^{13}C, and ^{15}N $T_{1\rho}$ values. ^{1}H and ^{13}C $T_{1\rho}$ values showed a pulse field strength dependence, but ^{15}N $T_{1\rho}$ did not. Assuming a two-site exchange process, an exchange time constant of 20−300 μs was estimated for the first adenosine in the CAA sequence. The exact nature of this motion remains unknown.

Genetic information may be encoded within the DNA sequence using its base pairing hydrogen bonds, functional groups, three-dimensional structure, and dynamics. DNA structure depends on the sequence, and some special sequences adopt unique conformations. On the other hand, little is known about the sequence dependence of DNA dynamics, in particular, on the nanosecond-to-picosecond time scale (*1*−*5*). The millisecond-to-microsecond time scale motion has been extensively studied for the TpA step (*6*−*12*) but not for other sequences. The base pair lifetime is another indicator of DNA motion, but only two special conformations, A-tract and Z-DNA, have been found to have a base pair lifetime differing substantially from other DNA duplex conformations (for review see ref *13*).

In this paper, we focus on the dynamics of two DNA sequences, which are known to have unique features of three-dimensional structure and dynamics: A-tracts and CpA·TpG steps. A-tract is a run of three or more consecutive adenosine (or thymidine) nucleotides. Such sequences are found in many bent sequences and some stable nucleosomes; they are involved in the regulation of transcriptional activation and termination. The three-dimensional structure of A-tracts has been extensively studied by many approaches, but the mechanism causing its curvature still is not known well (e.g., for review see ref *14*). The nanosecond-to-picosecond time scale motion of a short A-tract is no different from that of other DNA sequences (*3*, *15*). To date, the millisecond-to-microsecond time scale motion of A-tracts has been only reported for the T_nA_n junctions (*6*−*10*, *16*). The base pair lifetime for A-tracts (40−120 ms) is 10−30 times longer than that of a typical AT pair (4 ms) (*17*).

CpA steps have two distinct subgroups of conformations found in crystalline B-DNA, denoted CA^+ and CA^- (*18*). The CA^- conformation is characterized by unusually large values of slide (>2.5 Å) and twist (≈50°) with negative roll, in contrast to CA^+ with relatively small twist (≈30°) and positive roll. The CA^+ conformation is the predominant form. When the CpA step is situated at the 5′-end of an A-tract, DNA curvature is strongly enhanced (*19*). CpA steps have

† This work was supported by Grant GM39247 from the National Institutes of Health to T.L.J. and by Grant-in-Aid for Basic Scientific Research, Category B (No. 09480176), from the Ministry of Education, Science and Culture, Japan, and a grant from CREST (Core Research Evolutional Science and Technology) of the Japan Science and Technology Corp. (JST) to M.K. C.K. was supported in part by a long-term fellowship from the Human Frontier Science Program (Strasbourg, France).

* To whom correspondence should be addressed. Phone: (415) 476-1916. Fax: (415) 502-4690. E-mail: james@picasso.ucsf.edu.

‡ University of California, San Francisco.

§ CREST.

|| Tokyo Metropolitan University.

10.1021/bi0103260 CCC: $20.00
Published on Web 05/22/2001

been recognized as the most variable steps in DNA−protein complexes (*20*−*22*). These structural features suggest structural flexibility at the CpA step; however, no special motion on either nanosecond-to-picosecond or millisecond-to-microsecond time scales has been previously reported. Detection of molecular motions on these time scales, of course, is an indication that the barrier between conformations is not too high—there is not a large barrier to overcome in converting from one conformation to another.

Here, the millisecond-to-microsecond time scale motion of a DNA oligomer, d(CATTTGCATC)·d(GATGCAAATG), is analyzed on the basis of the rf[1] pulse field and magnetic field dependence of ^{1}H and ^{13}C transverse relaxation rates and the temperature dependence of several ^{15}N relaxation rates. For these experiments, every adenosine and guanosine was randomly fractionally enriched with 15% ^{13}C and 98% ^{15}N stable isotopes. This sequence has three CpA steps, and one is found at the 5′-end of a short A-tract. Thus it is possible to compare the motion of CpA steps with and without the neighboring A-tract. Previously, the solution structure of this DNA duplex was well characterized, and its rotational correlation time and other model-free dynamics parameters have been determined for most ^{1}H−^{13}C bonds in the purine residues (*3*, *23*−*25*).

EXPERIMENTAL PROCEDURES

Sample Preparation. A DNA duplex, d(^{1}C^{2}A^{3}T^{4}T^{5}T^{6}G^{7}-C^{8}A^{9}T^{10}C)·d(^{11}G^{12}A^{13}T^{14}G^{15}C^{16}A^{17}A^{18}A^{19}T^{20}G), containing 15% ^{13}C- and 98% ^{15}N-enriched adenosine and guanosine at each position, was prepared as described previously (*3*). The numbering system is shown on the left shoulder of the sequence. An unlabeled DNA duplex with identical sequence was prepared by annealing the equivalent concentrations of each strand (purchased from Espec Oligo Service Co., Tsukuba, Japan). Counterions were exchanged by adding 2 M NaCl, and excess salts and single strands were removed by gel filtration HPLC chromatography as described (*26*). NMR samples had a duplex concentration of about 1 mM in 10 or 20 mM phosphate buffer (pH 6.8) with 100 mM NaCl and 0.1 mM EDTA. The solvents were 90% H_2O/10% D_2O and 100% D_2O for the ^{13}C/^{15}N-labeled and unlabeled samples, respectively.

NMR Measurements. All NMR measurements for the ^{13}C/^{15}N-enriched sample were carried out on a Varian Inova-600 NMR spectrometer operating at 600 MHz ^{1}H frequency. The ^{15}N longitudinal relaxation rate R_1, ^{15}N transverse relaxation rate R_2, and ^{15}N{^{1}H} heteronuclear NOE were measured at three temperatures, 10, 20, and 30 °C, using standard 1D pulse sequences (*27*). The transverse and longitudinal cross-correlated relaxation rates between ^{15}N chemical shift anisotropy and ^{15}N−^{1}H dipolar interaction, η_Z and η_{XY}, respectively, were measured at 30 °C following the procedure reported for ^{13}C (*25*). The pulse repetition delay time was 2.5 s. Each relaxation data set was recorded with the following relaxation delay times: 50, 100, 150, 200, 250, 300, 350, 400, 500, 600, 700, and 800 ms for ^{15}N R_1; 0, 16, 32, 48, 64, 80, 96, 112, 128, 144, 160, and 176 ms for ^{15}N R_2; 60, 90, and 120 ms for ^{15}N η_Z; 30, 45, and 60 ms for ^{15}N η_{XY}. The ^{15}N{^{1}H} heteronuclear NOE was derived from the intensity ratio measured with and without 3 s proton presaturation.

The magnetic field strength dependence of ^{1}H T_2 was examined using the unlabeled sample at 25 °C on Bruker DRX500, DRX600, and DRX800 NMR spectrometers operating at 500, 600, and 800 MHz ^{1}H frequency, respectively. The ^{1}H T_2 data set was obtained using a Carr−Purcell−Meiboom−Gill (CPMG) spin−echo sequence, $(-\tau_{CPMG}-180°_y-\tau_{CPMG}-)_n$ (*28*, *29*), where τ_{CPMG} = 2.5 ms. The pulse repetition delay time was 15 s with the following relaxation delay times: 0, 10, 20, 30, 40, 50, 100, 150, and 200 ms.

The effect of the chemical exchange term on ^{1}H, ^{13}C, and ^{15}N transverse relaxation rates for the ^{13}C/^{15}N-enriched sample was investigated under the spin-locked field (*3*, *30*, *31*). 2D HSQC spectra were used for measuring ^{1}H and ^{13}C $T_{1\rho}$. Values for the spin-lock center frequency and pulse field strength were varied at 30 °C for ^{1}H and ^{13}C and at 10, 20, and 30 °C for ^{15}N. The "like" spin $T_{1\rho}$ was measured for ^{1}H (*31*). Six, three, and one spin-lock offset frequencies for ^{1}H, ^{13}C, and ^{15}N, respectively, were used with one to seven pulse field strengths as follows: 972, 1914, 4237, and 8143 Hz for ^{1}H at 6.19 ppm; 633, 1064, 2083, 4237, and 10 823 Hz for ^{1}H at 7.85 ppm; 471, 973, 1914, 3906, and 8143 Hz for ^{1}H at 8.19 ppm; 543, 1073, 2174, 4237, and 8772 Hz for ^{1}H at 9.52 ppm; 4237 Hz for ^{1}H at 11.19 and 14.52 ppm; 625, 735, and 1190 Hz for ^{13}C at 127 ppm; 1190, 2272, and 4544 Hz for ^{13}C at 133 ppm; 625 Hz for ^{13}C at 141 ppm; 625, 781, 1042, 1471, 1923, 2778, and 3846 Hz for ^{15}N at 198 ppm. The pulse repetition delay times were 1.5, 1.5, and 2.5 s for ^{1}H, ^{13}C, and ^{15}N, respectively. Each relaxation data set was obtained with the following relaxation delay times: 8, 16, 24, 40, 56, and 72 ms for ^{1}H and ^{13}C $R_{1\rho}$ (=$1/T_{1\rho}$); 16, 32, 48, 64, 80, 96, 112, 128, 144, 160, and 176 ms for ^{15}N $R_{1\rho}$. The ^{1}H T_1 was determined by the reported procedure (*3*) with delay times of 40, 80, 120, 160, 200, 250, and 300 ms. The ^{13}C T_1 values were taken from our previous report (*25*). These T_1 values were used to estimate the off-resonance contribution to ^{1}H and ^{13}C $R_{1\rho}$.

NMR Data Processing. All NMR data were processed on SUN SPARCstation 2, SGI Indigo R5000, or SGI O2 R10000 workstations using the following software: nmrPipe (NIH, Bethesda) (*32*), SPARKY 3 (*33*) (see http://www.cgl.ucsf.edu/home/sparky), and Felix (Molecular Simulation Inc.). Least-squares fitting with KaleidaGraph 3.0 (Abelbeck Software) was used to extract relaxation rates, assuming a monoexponential decay of peak heights with two parameters ($y = Ae^{-Bx}$). The model-free approach was used for the relaxation rate analysis of the imino ^{1}H−^{15}N system following previous reports (*3*, *34*, *35*). For most calculations, including the model-free approach, Microsoft Excel 98 (Microsoft Corp.) was used with the solver add-in function.

[1] Abbreviations: 1D, one dimensional; 2D, two dimensional; rf, radio frequency, T_1, spin−lattice relaxation time; $T_{1\rho}$, spin−lattice relaxation time in the rotating frame; T_2, spin−spin relaxation time; NOESY, nuclear Overhauser enhancement spectroscopy; NOE, nuclear Overhauser enhancement; R_1, spin−lattice relaxation rate; $R_{1\rho}$, spin−lattice relaxation rate in the rotating frame; R_2, spin−spin relaxation rate; η_Z, longitudinal cross-correlated relaxation rate between ^{15}N chemical shift anisotropy and ^{15}N−^{1}H dipolar interaction; η_{XY}, transverse cross-correlated relaxation rate between ^{15}N chemical shift anisotropy and ^{15}N−^{1}H dipolar interaction; HSQC, heteronuclear single-quantum coherence; CSA, chemical shift anisotropy.

RESULTS

^{15}N Relaxation Studies of Guanosine Imino Groups. The ^{15}N relaxation rates of imino NH groups for G6 and G14 residues were measured and subjected to the model-free analysis at three temperatures: 10, 20, and 30 °C. For the terminal residues G11 and G20, the imino signals were broadened and not observed clearly due to fast exchange with bulk water, especially at higher temperatures, so they were not studied here. Five relaxation parameters, measured as described in the Experimental Procedures section, are listed in Table 1. The overall correlation times (at three different temperatures) were determined previously for this DNA duplex from ^{13}C T_1/T_2 ratios (*25*). The experimental relaxation parameters were subjected to the model-free analysis (*34*); results deduced for the order parameter S^2 and internal motion correlation time τ_i are also listed in Table 1. When the longitudinal and transverse cross-correlated relaxation rates (η_Z and η_{XY}, respectively) were included in the analysis together with other relaxation parameters, the spectral density ratio relationship $J(0)/J(\omega_N) = 0.75(2\eta_{XY}/\eta_Z - 1)$ was used as input following a reported procedure (*25*). Anisotropy in the overall molecular tumbling was not included in the model-free analysis, because effects of anisotropy have not been detected for this oligomer (*3*). Also, the chemical exchange term was not included in the analysis, because its contribution was found to be negligible, as explained below.

The data at 30 °C were subjected to model-free dynamics analysis in two different combinations: including or excluding the observed cross-correlated relaxation rates η_Z and η_{XY}. The results were almost identical (S^2 within 0.01 and τ_i within 1 ps). Since the transverse cross-correlated relaxation rates do not have the exchange term contribution intrinsically (*25*, *36*), such a contribution to other relaxation parameters must be negligible for our system (otherwise, the results of the two calculations would be different). At the two lower temperatures, cross-correlated relaxation rates were not measured. In general, the chemical exchange term decreases with temperature, so data obtained at lower temperatures should have a negligible contribution from exchange.

The CSA value for 2′-deoxyguanosine N1 is required for the relaxation rate analysis (*3*, *34*, *35*). The ^{15}N CSA value $\Delta\sigma = \sigma_{11} - (\sigma_{22} + \sigma_{33})/2 = -120$ ppm was recently determined using the principal values from a solid-state NMR study of 2′-deoxyguanosine: $\sigma_{11} = 54$ ppm, $\sigma_{22} = 148$ ppm, and $\sigma_{33} = 201$ ppm (*37*). This value of −120 ppm is similar to the previously used value of −130 ppm (*38*). The chemical shift tensor is not axially symmetric, and the symmetry axis is not aligned to the N−H bond vector, so systematic errors are introduced to the determined model-free parameters. However, this effect is not great, because the dipolar contribution to relaxation is much greater than that of CSA. For example, the CSA contribution to R_1 and R_2 is about 13% in our case (14.1 T, decamer duplex, 10−30 °C range).

The observed ^{15}N R_1 rate increases and R_2 decreases with temperature (Table 1); this can be explained by the temperature dependence of the overall correlation time. The heteronuclear ^{15}N{^{1}H} NOE has a maximum at 20 °C. The temperature dependence of the determined order parameter is quite interesting, i.e., the order parameter of residue G14 is nearly constant but that of G6 rapidly decreases with temperature. A temperature dependence of the order parameter can be described by a characteristic temperature T^* of the dynamic process, using a relationship $d(1 - S)/dT = 3/(2T^*)$ (*39*). The T^* values for secondary structure elements, the loop, and the C-terminus of *Escherichia coli* ribonuclease HI were around 1000, 300, and 170 K, respectively (*39*). For the G6 residue, the T^* value is 336 K; thus its temperature dependence of the order parameter is comparable to that of the loop region of a protein. For G14, the T^* value could not be determined quantitatively, but it is expected to be fairly large since the derivative $d(1 - S)/dT$ is nearly zero, similar to secondary structure elements of a protein.

Table 1: Observed Imino ^{15}N Relaxation Rates and Model-Free Parameters Derived from These Rates[a]

temp (°C)	10	10	20	20	30	30
residue no.	6	14	6	14	6	14
R_1 (s^{-1})	1.48 (0.14)	1.48 (0.05)	1.98 (0.11)	1.80 (0.12)	1.94 (0.08)	2.28 (0.07)
R_2 (s^{-1})	9.57 (0.34)	7.76 (0.21)	6.09 (0.27)	4.98 (0.13)	4.74 (0.20)	4.40 (0.14)
NOE	0.62 (0.05)	0.64 (0.03)	0.79 (0.08)	0.78 (0.07)	0.59 (0.12)	0.59 (0.03)
η_Z (s^{-1})					3.39 (0.28)	3.54 (0.24)
η_{XY} (s^{-1})					6.37 (0.42)	6.71 (0.50)
τ_o (ns)[b]	5.03 (0.56)		3.89 (0.32)		3.02 (0.14)	
S^2	0.92 (0.03)	0.77 (0.02)	0.85 (0.03)	0.74 (0.02)	0.75 (0.03)	0.78 (0.02)
τ_i (ps)	214 (21)	55 (12)	19 (56)	14 (19)	44 (159)	110 (90)

[a] R_1, R_2, η_Z, and η_{XY} are the imino ^{15}N longitudinal and transverse relaxation rates and the longitudinal and transverse cross-correlated relaxation rates, respectively. NOE is the ^{15}N{^{1}H} heteronuclear NOE. S^2, τ_o, and τ_i are the generalized order parameter, overall correlation time, and correlation time for the internal motion, respectively. Experimental errors are shown in parentheses. Errors for S^2 and τ_i are evaluated by a Monte Carlo procedure using 100 synthetic data sets (*3*). [b] The overall correlation time is determined from the ^{13}C T_1/T_2 ratio (*25*).

Proton Line Width in NOESY Spectra. In a ^{1}H 1D spectrum of the unlabeled DNA sample, certain H8 resonances are somewhat broader than others. A NOESY spectrum previously acquired (*23*) was carefully revisited to estimate the ^{1}H line width quantitatively. The purine H8 and H2 signals do not have proton−proton *J*-couplings, so the apparent line widths in the ω_2 dimension in a NOESY spectrum are simply related to their apparent T_2. Each NOESY cross-peak was individually line-fitted with the SPARKY software (*33*). The range of the line width in the ω_2 dimension is 5−9 Hz; most signals are observed within a quite narrow range, i.e., 7 ± 1 Hz. Table 2 shows the average values for the purine H8 protons. The line widths of H8 protons in A16 and A17 are clearly increased compared to other residues. There is some hint that the H8 line width for the A18 residue is also somewhat larger but perhaps not significantly so. A similar trend was observed for the H8 line widths in the same NOESY spectrum processed with an exponential window function (data not shown).

A similar analysis for the adenine H2 line widths was less conclusive, because only a small number of cross-peaks were suitable for quantitative line fitting. Consequently, no further analysis of adenine H2 signals will be considered here.

The apparent line width has contributions from the intrinsic line width, chemical exchange, and static magnetic field inhomogeneity. The magnetic field inhomogeneity contribu-

Table 2: Purine H8 Resonance Line Widths (Hz)[a]

residue	average	std[b]	delta[c]	number[d]
A2	6.9	0.21	−0.2	11
A8	6.5	0.24	−0.6	11
A12	6.9	0.17	−0.2	11
A16	8.2	0.23	1.1	8
A17	7.8	0.27	0.7	6
A18	7.1	0.26	0.0	9
adenine	7.1	0.61		56
G6	7.0	0.37	0.4	12
G11	6.2	0.34	−0.4	7
G14	6.7	0.32	0.1	12
G20	6.1	0.28	−0.5	8
guanine	6.6	0.48		39

[a] A NOESY spectrum was processed with a Gaussian window function with zero-filling to a digital resolution of 2.15 Hz per data point. Individual cross-peaks were fitted with a 2D Gaussian function using SPARKY software (*33*). The line width in the ω_2 dimension was averaged for each nucleus or for a group of nuclei. [b] Standard deviation. [c] Difference between the average line width for a particular nucleus and the average for the corresponding group. [d] Number of cross-peaks.

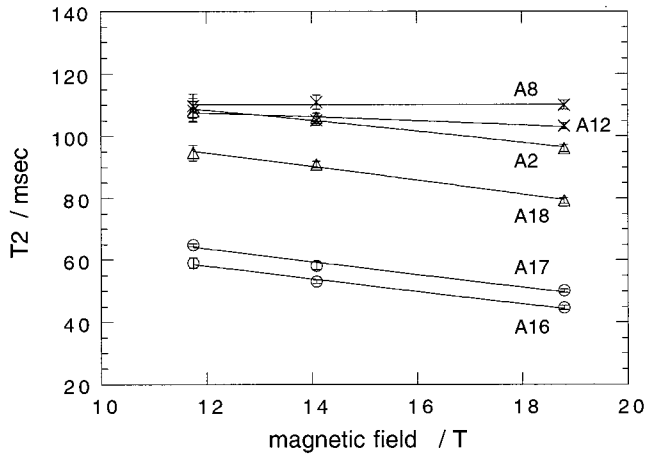

FIGURE 1: Magnetic field dependence of proton T_2 for all adenosine H8 signals at 25 °C. Assignments and error bars are given in the figure. Fitted lines were calculated from the relation $T_2^{-1} \propto B_0^2$ (eq 4); T_2(dipole) and b/a were used as adjustable parameters.

tion is uniform for all signals. However, the intrinsic line width and the exchange contributions both depend on DNA sequence. Thus the apparent broadening of H8 signals observed for A16 and A17 residues cannot be assigned a priori to the intrinsic or the exchange contribution. In fact, this DNA molecule is kinked in the base pair step T5-G6•C15-A16 (*24*); this may change the intrinsic line width. For unambiguous detection of an exchange process, other approaches are required. As described below, these other approaches could entail monitoring the pulse and magnetic field strength dependence of $T_{1\rho}$ or T_2 for the base ^{1}H, ^{13}C, and ^{15}N nuclei, in particular, for the H8 and C8 signals.

Magnetic Field Dependence of ^{1}H T_2. The static magnetic field dependence of line widths or of T_2 is one method to detect millisecond-to-microsecond time scale motions. The measured or apparent transverse relaxation rate R_2 ($=1/T_2$) can have a contribution from exchange. The term R_{ex} reflects the contribution of chemical exchange effects to the transverse relaxation rate:

$$R_2 = R_2(\text{dipole}) + R_{ex} \quad (1)$$

where R_2(dipole) is the transverse relaxation rate due solely to dipole−dipole relaxation, i.e., in the absence of chemical exchange. Conformational fluctuations on the microsecond-to-millisecond time scale are traditionally considered to be chemical exchange. Assuming exchange between two sites, A and B, the exchange term R_{ex} is expressed analytically as (*40*)

$$R_{ex} = (\delta\omega)^2 p_A p_B \tau_{ex}/(1 + \tau_{ex}^2 \omega_e^2) \quad (2)$$

where p_A and p_B are the populations of states A and B, respectively; $\delta\omega = \omega_A - \omega_B$ is the chemical shift difference between the two sites; τ_{ex} is the time constant of the exchange process; $\omega_e = (\omega_1^2 + \Delta\omega^2)^{1/2}$ is the effective field; ω_1 is the spin-lock field strength; ω is the spin-lock rf frequency; ω_0 = ($2\pi \times$ resonance frequency); and $\Delta\omega = \omega - \omega_0$ is the reduced static field, i.e., is $2\pi \times$ off-resonance frequency.

For on-resonance signals, the exchange term R_{ex} increases quadratically with the magnetic field strength B_0 through the $(\delta\omega)^2$ term (eq 2). Millet et al. (*41*) have carefully analyzed the magnetic field dependence of the exchange term R_{ex} and found that it can be expressed by a scaling factor α: $\delta R_{ex}/R_{ex} = \alpha\delta B_0/B_0$, $\alpha = \text{d}(\ln R_{ex})/\text{d}(\ln \delta\omega)$, where $0 < \alpha < 2$ for $p_A > 0.7$. They concluded that quadratic scaling of the exchange term R_{ex} is obtained only for the limit of $\alpha = 2$, which is very fast exchange; such an assumption is not tenable for most cases. The quadratic dependence of the R_{ex} term may be too strong; nevertheless, the R_{ex} term always increases with B_0 even in the case of an intermediate or slow exchange process, because the α value is positive. As shown in eq 1, the apparent T_2 relaxation rate consists of the intrinsic dipolar relaxation contribution and the exchange contribution. Generally, the dipolar relaxation rate decreases and the exchange rate increases when B_0 increases. If the exchange term is negligible, the apparent ^{1}H T_2 value is nearly constant or increases slightly with B_0. If the exchange term is significant, then the apparent ^{1}H T_2 value decreases. Equation 1 consequently can be modified; the decrease of apparent T_2 is related to the order of the magnetic field strength dependence, α, through the relation

$$T_2(\text{apparent}) = 1/[R_2(\text{dipole}) + R_{ex}] = 1/[a + bB_0^{\alpha}] \quad (3)$$

where a and b are variable coefficients. The dipolar contribution is assumed to be independent of B_0 in the above equation. In the case of very fast exchange, $\alpha = 2$.

The apparent ^{1}H T_2 values were determined at 25 °C for all adenosine H8 signals of the unlabeled sample at ^{1}H frequencies of 500, 600, and 800 MHz. The experimental error was 1−3% and less than 0.4 ms. Other proton signals were not analyzed. In Figure 1, the apparent T_2 values are plotted as a function of the static magnetic field strength. The apparent T_2 values of H8 signals for the A16 and A17 residues are significantly smaller than the others, and that of A18 is somewhat smaller, at all three magnetic field strengths. These results are consistent with our analysis of ^{1}H line widths in the NOESY spectrum (Table 2). For two residues, A8 and A12, the T_2 values do not depend on the magnetic field. For the other four residues (A2, A16, A17, and A18), the differences between the apparent T_2 values recorded at 500 and 800 MHz amount to 12−16 ms. The magnitude of the apparent T_2 value is different for each residue, so the apparent $R_2 = 1/T_2$(apparent) is preferred for the comparison. The differences in apparent R_2 at 500 and

800 MHz were 1.1, 5.4, 4.5, and 2.1 s^{-1} for A2, A16, A17, and A18, respectively. For the A16 and A17 residues, the observed differences are large, but for the other two residues, they are comparatively small. These differences in the apparent R_2 values can be confidently attributed to an exchange process manifest at H8 positions, although the magnitude of the exchange differs somewhat for each residue.

From the static magnetic field strength dependence of the apparent ^{1}H T_2, the intrinsic dipolar relaxation contribution to the apparent T_2 was estimated assuming $R_{ex} = bB_0^2$ (similar to eq 3), where the apparent T_2 value is expressed as

$$T_2(\text{apparent}) = 1/(R_2 + R_{ex}) = 1/(a + bB_0^2) = T_2(\text{dipole})/(1 + (b/a)B_0^2) \quad (4)$$

The best-fit curve shown in Figure 1 was obtained for each residue with a correlation coefficient greater than 0.99; T_2(dipole) and b/a were used as adjustable parameters. Under our simple assumption, T_2(dipole) is independent of the magnetic field, and consequently it was determined as a limiting value at $B_0 = 0$. T_2(dipole) values were determined to be 118, 110, 111, 74, 79, and 109 ms for A2, A8, A12, A16, A17, and A18, respectively. Excepting A16 and A17 residues, the other four values are similar to each other; this might reflect the similarity of local structure and dynamics for these residues. As mentioned above, the quadratic magnetic field strength dependence was not very reliable theoretically (*41*). Actually, a quadratic dependence was not proven in our analysis either; a linear dependence can also explain our experimental data quite well, judging from the correlation coefficients.

rf Pulse Field Strength Dependence of ^{1}H, ^{13}C, and ^{15}N $T_{1\rho}$. In our studies cited above, the ^{15}N relaxation data from the imino group of G6, proton line width values for H8 protons of A16 and A17 (and possibly A18), and magnetic field dependence of H8 proton transverse relaxation time measurements for A16 and A17 (with a diminished dependence for A18) all indicate that there are some conformational fluctuations (chemical exchange) in the millisecond-to-microsecond time regime for the CAA·TTG moiety of the decamer duplex. However, the above data do not allow estimation of the time constant of the exchange process. Such millisecond-to-microsecond time scale motions can also be studied by the pulse field strength dependence of $T_{1\rho}$. In principle, this can even yield quantitative exchange rates.

The observed relaxation rate $R_{1\rho}$ ($=1/T_{1\rho}$) consists of an on-resonance term ($R_2 \sin^2\theta$), exchange term ($R_{ex} \sin^2\theta$), and off-resonance term ($R_1 \cos^2\theta$) (*40*, *42*):

$$R_{1\rho} = (R_2 + R_{ex}) \sin^2\theta + R_1 \cos^2\theta \quad (5)$$

where $\theta = \arctan(\omega_1/\Delta\omega)$ is the angle between the directions of the static field and the effective field ω_e (see definitions of ω_e, ω_1, and $\Delta\omega$ in the previous section). In principle, any off-resonance contributions can be taken into account using eq 5 with the assumption $\omega_e\tau_o \ll 1$, where τ_o is the rotational correlation time of the molecule. The ω_e value increases with the off-resonance frequency $\Delta\omega = \omega - \omega_0$.

Practically, the τ_{ex} value can be quantitatively determined from the relationship between the observed $R_{1\rho}$ and ω_e, using eqs 2 and 5, although the other terms, $\delta\omega$, p_A, and p_B, are not determined individually. Equations 2 and 5 are combined as

$$(R_{1\rho} - R_1 \cos^2\theta)/\sin^2\theta = R_2 + (\delta\omega)^2 p_A p_B \tau_{ex}/(1 + \tau_{ex}^2\omega_e^2) \quad (6)$$

The ω_e and θ values were experimentally controlled by the ω_1 and $\Delta\omega$ values, i.e., by setting the pulse field strength and spin-lock rf frequency. The R_1 and $R_{1\rho}$ values were determined for the ^{1}H, ^{13}C, and ^{15}N nuclei of the doubly labeled sample, as described in the Experimental Procedures section, by fitting signal decays to exponentials. Finally, the experimental data were fitted to eq 6, using R_2, $(\delta\omega)^2 p_A p_B$, and τ_{ex} as adjustable parameters.

The chemical shift difference between the imino ^{15}N signals for G6 and G14 residues is less than 0.2 ppm (=12 Hz at 600 MHz ^{1}H frequency), so the off-resonance contribution to the ^{15}N $R_{1\rho}$ was neglected. For other nuclei, the off-resonance term was calculated from the value of ω_1 determined from the 90° pulse length, $\Delta\omega$ calculated from the frequency difference between the instrument's carrier frequency and the observed signal's frequency, and R_1 recorded by independent experiments. Considering the limitation $\omega_e\tau_o \ll 1$ in eq 5, the range of ω_e values must be less than 100 kHz since the overall correlation time of our sample is about 3−5 ns. With our experimental conditions, this limitation is satisfied, because ω_1 and $\Delta\omega$ are less than 11 and 45 kHz, respectively.

For the ^{1}H $R_{1\rho}$ measurements, six spin-lock offsets combined with four to five pulse field strengths were used to detect the exchange term R_{ex} at 30 °C. The off-resonance contribution was corrected using eq 5 and the longitudinal relaxation rate R_1 determined by nonselective pulses. However, the longitudinal relaxation of ^{1}H can be a multiexponential decay process unless a selective pulse is used. Our $R_{1\rho}$ measurements used the spin-lock pulse with a wide variety of pulse field strengths; under such conditions the R_1 contribution to $R_{1\rho}$ is not defined experimentally and theoretically. That is, the apparent R_1 differs from the true R_1, which could be obtained using a selective pulse. Thus for ^{1}H $R_{1\rho}$ (eq 5), the off-resonance correction ($R_1 \cos^2\theta$) in the expression is potentially useful but is not very reliable. Here we used a limited set of the ^{1}H $R_{1\rho}$ values where the off-resonance contribution was small ($\cos^2\theta \leq 0.15$), since the accuracy and precision of the R_1 value have big impacts on the $R_2 + R_{ex}$ term when the off-resonance contribution is large. In fact, when all data were used for the analysis, no clear relationship was obtained between the corrected $R_{1\rho}$ values and the effective field strengths ω_e. For the final analysis, two spin-lock offsets and three or four pulse field strengths were used as follows: 1064, 2083, 4237, and 10 823 Hz at 7.85 ppm; 1914, 3906, and 8143 Hz at 8.19 ppm. With these field strengths, the on-resonance condition ($\cos^2\theta \leq 0.01$) was satisfied for most proton signals. A systematic decrease of the ^{1}H $R_{1\rho}$ value with increasing effective field was observed for proton H8 of the A16 residue as shown in Figure 2A. The dotted line shown is the best-fit curve obtained using the parameters $(\delta\omega)^2 p_A p_B = (4 \pm 9) \times 10^5$ and $\tau_{ex} = 18 \pm 16$ μs. Since the $p_A p_B$ term is always smaller than 0.25, $\delta\omega$ is greater than 1239 s^{-1} = 197 Hz (=0.3 ppm at 600 MHz). Although a systematic decrease is

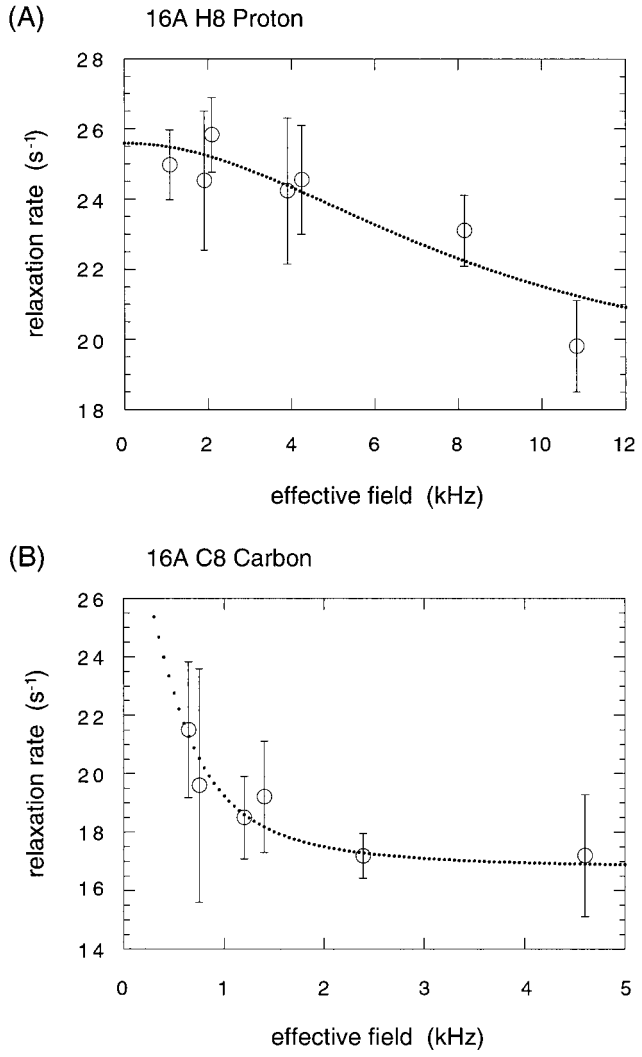

FIGURE 2: Pulse field dependence of the transverse relaxation rate for the H8 proton (A) and C8 carbon (B) of A16 at 30 °C. Error bars represent fitting errors obtained in each relaxation rate determination. The dotted line is the best fit to the observed data assuming fast exchange between two sites (see text).

evident, values for these parameters obviously have a large error since the experimental data points are scattered. Other H8 and H2 signals did not show such a systematic decrease in their ^{1}H $R_{1\rho}$ values.

For the ^{13}C $R_{1\rho}$ measurements, three spin-lock offsets combined with three pulse field strengths were used at 30 °C. The off-resonance contribution was corrected from eq 5 using the longitudinal relaxation rate R_1. In contrast to ^{1}H, the ^{13}C longitudinal relaxation is a single-exponential process for this sample (*3*). Although the R_1 values were determined reliably, the R_{ex} value still could not be determined accurately when the chemical shift offset term $\Delta\omega$ was large. Therefore, only two spin-lock offsets were used for the analysis of C2 and C8 signals as follows: 625, 735, and 1190 Hz for C8 at 127 ppm; 1190, 2272, and 4544 Hz for C2 and C8 at 133 ppm; 625 Hz for C2 at 141 ppm. A systematic decrease in the ^{13}C $R_{1\rho}$ for the C8 signal of the A16 residue was observed when increasing the effective field ω_e (Figure 2B). Other C8 and C2 signals did not show such a systematic decrease. The dotted line shown is the best fit obtained using the parameters $(\delta\omega)^2\, p_A p_B = (38 \pm 13) \times 10^3$ and $\tau_{ex} = (3 \pm 4) \times 10^2$ μs. The $\delta\omega$ value is greater than 390 rad·s^{-1} (=62 Hz = 0.4 ppm at 150 MHz). The systematic decrease is clear here, and the decay is quite fast. The difference of the decay rate between ^{13}C and ^{1}H $R_{1\rho}$ leads to some discrepancy in the time constants determined for the exchange process, τ_{ex} (302 and 18 μs for carbon and proton, respectively). The difference in the $\delta\omega$ values is quite small on the chemical shift scale of ^{13}C and ^{1}H. Although the errors in values determined for $(\delta\omega)^2 p_A p_B$ and τ_{ex} are undoubtedly substantial for both ^{13}C and ^{1}H (30−230%), it is clear nevertheless that an exchange process occurs in this time regime and is localized to only part of the decamer, including at least the C8H8 group of the A16 residue.

For the ^{15}N $R_{1\rho}$ measurements, seven pulse field strengths were used at 10, 20, and 30 °C. The $R_{1\rho}$ values determined were independent of the pulse field strength (data not shown). A small but systematic decrease and increase in $R_{1\rho}$ were measured at the weakest and strongest pulse field strength of ω_1, respectively. Since the magnitude of this change is not very great, being found at the limiting field strengths only, these differences have not been analyzed further. This observation suggests the absence of a detectable exchange process on the millisecond-to-microsecond time scale, which affects $R_{1\rho}$ values for ^{15}N nuclei. An exchange process may be undetectable under any of the following conditions: the time constant for the exchange process τ_{ex} is too small; the population of one conformation is too small; or the chemical shift difference is too small. Under such conditions there is no incentive to infer a second conformation exchanging on the millisecond-to-microsecond time scale, based on the ^{15}N $R_{1\rho}$ data, even though the T_2 value of the imino nitrogen of G6 strongly suggests that there is some additional motion.

DISCUSSION

Slow Molecular Motion in the CAA·TTG Sequence. A number of special features have been reported for the G6 residue within the CAA·TTG sequence. For example, the H/D exchange rate at position 8 is faster than in other residues (*3*); the DNA helix is kinked at the TpG step, and two stable conformations were found for the α and γ dihedral angles (*24*). In the present work, the G6 residue was found to have a strong temperature dependence of the order parameter S^2 for the imino NH group (Table 1). From the characteristic temperature analysis, the temperature dependence of S^2 is comparable to that of a protein loop region (*39*). Such a temperature dependence was found only for the G6 residue but not for G14. The experimental data in Table 1 show that this difference is manifest in the ^{15}N T_2 value, which leads to the diminished value of S^2 for G6. This implies that a slow and presumably localized motion exists at the G6 residue. Its time scale could not be determined from our data, because the ^{13}C and ^{15}N $T_{1\rho}$ values for this residue did not show any significant pulse field strength dependence. As mentioned above, $T_{1\rho}$ data may not necessarily reveal conformational exchange, if the exchange is too fast, the population of one of the conformers is too small, or the chemical shift difference between the conformers is too small. In addition, the ^{13}C R_1, R_2, and NOE values of the G6 residue at base C8H8 positions (2.35 s^{-1}, 18.05 s^{-1}, and 0.94, respectively) are systematically smaller than the average values for other purine residues (2.55 s^{-1}, 18.90 s^{-1}, and 1.11, respectively) (*3*); thus a small decrease in the T_2 value induced by the exchange process may also be below

detection. The temperature dependence of the order parameters has not been carried out in this work for base CH groups; it is possible that they have a tendency similar to that of the imino NH group for the G6 residue.

Chemical exchange, i.e., millisecond-to-microsecond time scale motion, was indicated by the apparent H8 proton line broadening for the two adenosine residues in the CAA·TTG sequence (Table 2). For the A16 residue, the first adenosine in the CAA region, the time constant of the exchange process was estimated to be 20−300 μs by the pulse field strength dependence of ^{1}H and ^{13}C $T_{1\rho}$. Taken alone, the apparent line broadening for A17, the second adenosine in the CAA region, could be explained by another factor, such as structure-dependent variation of the intrinsic line width. However, the strong static magnetic field dependence of ^{1}H T_2 supports the presence of the exchange process for A17 (Figure 1), and this residue does not have special features in its structure and picosecond-to-microsecond time scale dynamics (*3*, *24*). Therefore, the detected apparent line broadening for A17 must be due to the chemical exchange process. Additionally, adenosine H8 NOE cross-peaks in the CAAAT·ATTTG region are broader than in other residues (Table 2), and these adenosine H8 T_2 values are smaller than others at all field strengths as well as decrease with increasing magnetic field strength (Figure 1). Although the H8 T_2 relaxation time of the adjacent A2 residue exhibits a magnetic field dependence as well as those of residues A16, A17, and A18, its T_2 value is not as low as the sequential three. We suggest that the slow motion is more pronounced at the first adenosine in the CAA·TTG sequence, but its effect extends over the CAAAT·ATTTG region. To confirm this conclusion, pyrimidine residues need to be studied using a sample with these residues enriched with ^{13}C and ^{15}N isotopes.

Comparison of the Three CpA/TpG Steps in the Decamer Duplex. The pyrimidine−purine dinucleotide step can have many conformations compared to other sequences (for example, see ref *57*). The CpA dinucleotide step in particular is very polymorphic, not only in free DNA but in DNA−protein complexes (see introduction). Figure 3 illustrates the extent of conformational space found for CpA steps. Here, 23 conformations of the CpA step are shown which have been found in 14 B-DNA crystal structures without bound drugs or proteins (*18*). In this figure, the AT pairs are superimposed and shown on the top or surface side. Comparing the top figure to the bottom, it is clear that the conformational space for the CpA steps is anisotropic. Specifically, the position of base pairs varies significantly within the given base plane. In these structures, the helical parameter slide covers a wide range, 0.8−2.7 Å, and helical twist covers a range of 31−49° (*18*). Clearly, CpA is flexible in the sense of possessing many different conformations in the crystalline state. However, whether such structural flexibility is reflected in local dynamics in solution has not been previously addressed. Of course, the exact nature of the slow motion observed in this work remains unknown; its elucidation would require a different approach (see, e.g., ref *43*). It also remains to be seen if conformations similar to the crystal CA$^-$ conformation are present in solution, at least as a minor conformer. In general, solution and crystal conformations of B-DNA are significantly different (*44*). In particular, high-resolution NMR structures do not show a high level of conformational heterogeneity for the CpA steps;

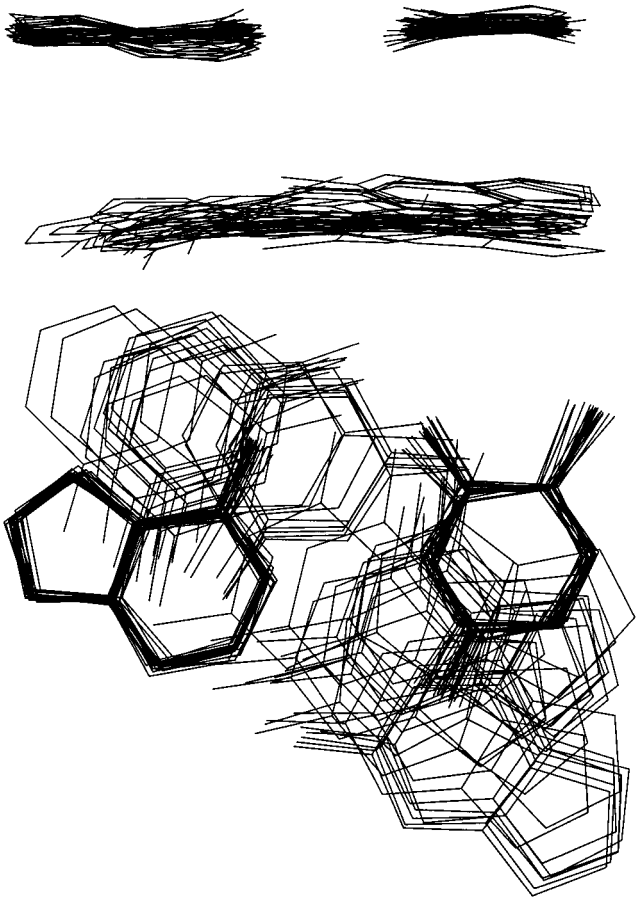

FIGURE 3: The 23 conformations of CpA dinucleotide steps found in crystal structures of 14 B-DNA duplexes lacking drugs or proteins (for a survey, see ref *18*). The following Nucleic Acid Database structures were utilized: BDJ008, BDJ017, BDJ019, BDJ051, BDJB27, BDJB43, BDJB44, BDL006, BDL007, BDL015, BDL028, BDL029, and BDL038 (*46*−*56*). (The Atlas of Nucleic Acid Containing Structures can be accessed at http://202.213.175.11/NDB/NDBATLAS/index.html.) The structures were superimposed using the heavy atoms of AT base pairs. They are viewed from the side (top figure) and along the helical axis (bottom figure). The bottom figure is obtained by a 90° rotation of the top figure.

on average, the solution CpA conformation is closer to the crystal CA$^+$ than to the crystal CA$^-$ conformation (*44*, *45*). However, solution NMR structures represent time- and ensemble-averaged conformations; perhaps some of these structures need to be revisited in light of evidence of conformational fluctuations.

Our sequence has three CpA steps. If all CpA steps were similar in dynamical flexibility, all three CpA steps would show common motional features. However, our results show the presence of microsecond-to-millisecond motion only for the CAA·TTG sequence, i.e., for only one CpA step—not the others. No slow motion has been reported for CpA steps in other sequences; our observation is the first of the kind. The CAA·TTG region is part of a larger CAAA·TTTG sequence in our oligomer, and it can be considered as a junction between the CpA step and a short A-tract. For T_nA_n sequences, exchange broadening is greater for the TAA sequence than for any other XpTpApX sequences (*11*). Thus some common mechanisms may exist for slow motion for both TpA and CpA steps at the 5′-end of A-tracts.

In conclusion, our experimental results indicate the presence of motion in the microsecond-to-millisecond range in

the CAA·TTG sequence of a DNA oligomer. Although each has significant experimental error, there are three independent lines of evidence for such motion. Slow motion in DNA duplexes was found at the TpA step more than 15 years ago (*6*−*10*, *16*). Thus the CAA·TTG sequence is the second example of slow motion. The TpA step and CAA·TTG sequence both have the pyrimidine−purine dinucleotide step where the purine base is adenine. The pyrimidine−purine step is considered to be flexible or unstable, and our data support such a notion for the CAA·TTG sequence. This is biologically important since both the TpA step and the CAA·TTG sequences are found in bent DNA segments implicated in the regulation of transcription. In this report, we do not discuss DNA bending mechanisms, but our results may very well pertain to this problem.

ACKNOWLEDGMENT

The authors are grateful to Dr. Akira Ono for a $^{13}C/^{15}N$-labeled sample, Dr. Kaoru Nomura for a helpful comment about CSA, and Dr. Rieko Ishima (NIH) for helpful discussion and for providing us with a preprint.

REFERENCES

1. Borer, P. N., LaPlante, S. R., Kumar, A., Zanatta, N., Martin, A., Hakkinen, A., and Levy, G. C. (1994) *Biochemistry 33*, 2441−2450.
2. Paquet, F., Gaudin, F., and Lancelot, G. (1996) *J. Biomol. NMR 8*, 252−260.
3. Kojima, C., Ono, A., Kainosho, M., and James, T. L. (1998) *J. Magn. Reson. 135*, 310−333.
4. Spielmann, H. P. (1998) *Biochemistry 37*, 16863−16876.
5. Spielmann, H. P. (1998) *Biochemistry 37*, 5426−5438.
6. Lefevre, J. F., Lane, A. N., and Jardetzky, O. (1985) *FEBS Lett. 190*, 37−40.
7. Lane, A. N. (1989) *Biochem. J. 259*, 715−724.
8. Schmitz, U., Sethson, I., Egan, W., and James, T. L. (1992) *J. Mol. Biol. 227*, 510−531.
9. Kennedy, M. A., Nuutero, S. T., Davis, J. T., Drobny, G., and Reid, B. R. (1993) *Biochemistry 32*, 8022−8035.
10. McAteer, K., Ellis, P. D., and Kennedy, M. A. (1995) *Nucleic Acids Res. 23*, 3962−3966.
11. McAteer, K., and Kennedy, M. A. (2000) *J. Biomol. Struct. Dyn. 17*, 1001−1009.
12. Lingbeck, J., Kubinec, M. G., Miller, J., Reid, B. R., Drobny, G. P., and Kennedy, M. A. (1996) *Biochemistry 35*, 719−734.
13. Guéron, M., and Leroy, J. L. (1995) *Methods Enzymol. 261*, 383−413.
14. Crothers, D. M., and Shakked, Z. (1999) in *Oxford Handbook of Nucleic Acids Structure* (Neidle, S., Ed.) pp 455−470., Oxford University Press, Oxford.
15. Michalczyk, R., Silks, L. A., III, and Russu, I. M. (1996) *Magn. Reson. Chem. 34*, S94−S104.
16. Lefevre, J. F., Lane, A. N., and Jardetzky, O. (1988) *Biochemistry 27*, 1086−1094.
17. Leroy, J.-L., Charretier, E., Kochoyan, M., and Guéron, M. (1988) *Biochemistry 27*, 8894−8898.
18. Gorin, A. A., Zhurkin, V. B., and Olson, W. K. (1995) *J. Mol. Biol. 247*, 34−48.
19. Nagaich, A. K., Bhattacharyya, D., Brahmachari, S. K., and Bansal, M. (1994) *J. Biol. Chem. 269*, 7824−7833.
20. Dickerson, R. E., and Chiu, T. K. (1997) *Biopolymers 44*, 361−403.
21. Olson, W. K., Gorin, A. A., Lu, X.-J., Hock, L. M., and Zhurkin, V. B. (1998) *Proc. Natl. Acad. Sci. U.S.A. 95*, 11163−11168.
22. El Hassan, M. A., and Calladine, C. R. (1998) *J. Mol. Biol. 282*, 331−343.
23. Weisz, K., Shafer, R. H., Egan, W., and James, T. L. (1992) *Biochemistry 31*, 7477−7487.
24. Weisz, K., Shafer, R. H., Egan, W., and James, T. L. (1994) *Biochemistry 33*, 354−366.
25. Kojima, C., Ono, A., Kainosho, M., and James, T. L. (1999) *J. Magn. Reson. 136*, 169−175.
26. Kyogoku, Y., Kojima, C., Lee, S. J., Tochio, H., Suzuki, N., Matsuo, H., and Shirakawa, M. (1995) *Methods Enzymol. 261*, 524−541.
27. Farrow, N. A., Muhandiram, R., Singer, A. U., Pascal, S. M., Kay, C. M., Gish, G., Shelson, S. E., Pawson, T., Forman-Kay, J. D., and Kay, L. E. (1994) *Biochemistry 33*, 5984−6003.
28. Carr, H. Y., and Purcell, E. M. (1954) *Phys. Rev. 94*, 630−635.
29. Meiboom, S., and Gill, D. (1958) *Rev. Sci. Instrum. 29*, 688−691.
30. Peng, J. W., Thanabal, V., and Wagner, G. (1991) *J. Magn. Reson. 95*, 421−427.
31. Ishima, R., Wingfield, P. T., Stahl, S. J., Kaufman, J. D., and Torchia, D. A. (1998) *J. Am. Chem. Soc. 120*, 10534−10542.
32. Delaglio, F., Grzesiek, S., Vuister, G. W., Zhu, G., Pfeifer, J., and Bax, A. (1995) *J. Biomol. NMR 6*, 277−293.
33. Goddard, T. D., and Kneller, D. G. (1998) SPARKY, Version 3, University of California, San Francisco.
34. Lipari, G., and Szabo, A. (1982) *J. Am. Chem. Soc. 104*, 4546−4559.
35. Kay, L. E., Torchia, D. A., and Bax, A. (1989) *Biochemistry 28*, 8972−8979.
36. Kroenke, C. D., Loria, J. P., Lee, L. K., Rance, M., and Palmer, A. G. (1998) *J. Am. Chem. Soc. 120*, 7905−7915.
37. Lorigan, G. A., McNamara, R., Jones, R. A., and Opella, S. J. (1999) *J. Magn. Reson. 140*, 315−319.
38. Akke, M., Fiala, R., Jiang, F., Patel, D., and Palmer, A. G. (1997) *RNA 3*, 702−709.
39. Mandel, A. M., Akke, M., and Palmer, A. G., III (1996) *Biochemistry 35*, 16009−16023.
40. Davis, D. G., Perlman, M. E., and London, R. E. (1994) *J. Magn. Reson. B 104*, 266−275.
41. Millet, O., Loria, J. P., Kroenke, C. D., Pons, M., and Palmer, A. G., III (2000) *J. Am. Chem. Soc. 122*, 2867−2877.
42. Akke, M., and Palmer, A. G., III (1996) *J. Am. Chem. Soc. 118*, 911−912.
43. Görler, A., Ulyanov, N. B., and James, T. L. (2000) *J. Biomol. NMR 16*, 147−164.
44. Ulyanov, N. B., and James, T. L. (1995) in *Methods in Enzymology* (James, T. L., Ed.) pp 90−120, Academic Press, New York.
45. MacDonald, D., Herbert, K., Zhang, X., Polgruto, T., and Lu, P. (2001) *J. Mol. Biol. 306*, 1081−1098.
46. Prive, G. G., Heinemann, U., Chandrasegaran, S., Kan, L.-S., Kopka, M. L., and Dickerson, R. E. (1987) *Science 238*, 498−504.
47. Prive, G. G., Yanagi, K., and Dickerson, R. E. (1991) *J. Mol. Biol. 217*, 177−199.
48. Goodsell, D. S., Kopka, M. L., Cascio, D., and Dickerson, R. E. (1993) *Proc. Natl. Acad. Sci. U.S.A. 90*, 2930−2934.
49. Nelson, H. C., Finch, J. T., Luisi, B. F., and Klug, A. (1987) *Nature 330*, 221−226.
50. Heinemann, U., and Alings, C. (1989) *J. Mol. Biol. 210*, 369−381.
51. DiGabriele, A. D., Sanderson, M. R., and Steitz, T. A. (1989) *Proc. Natl. Acad. Sci. U.S.A. 86*, 1816−1820.
52. Edwards, K. J., Brown, D. G., Spink, N., Skelly, J. V., and Neidle, S. (1992) *J. Mol. Biol. 226*, 1161−1173.
53. Lipanov, A., Kopka, M. L., Kaczor-Grzeskowiak, M., Quintana, J., and Dickerson, R. E. (1993) *Biochemistry 32*, 1373−1389.
54. Yoon, C., Prive, G. G., Goodsell, D. S., and Dickerson, R. E. (1988) *Proc. Natl. Acad. Sci. U.S.A. 85*, 6332−6336.
55. Narayana, N., Ginell, S. L., Russu, I. M., and Berman, H. M. (1991) *Biochemistry 30*, 4449−4455.
56. Larsen, T. A., Kopka, M. L., and Dickerson, R. E. (1991) *Biochemistry 30*, 4443−4449.
57. Dickerson, R. E. (1998) *Nucleic Acids Res. 26*, 1906−1926.

BI0103260